university of groningen

University Medical Center Groningen

University of Groningen

Decoupling the Amplitude and Wavelength of Anisotropic Topography and the Influence on Osteogenic Differentiation of Mesenchymal Stem Cells Using a High-Throughput Screening Approach

Yang, Liangliang; Ge, Lu; Zhou, Qihui; Jurczak, Klaudia Malgorzata; van Rijn, Patrick

Published in:
ACS Applied Bio Materials

DOI:
10.1021/acsabm.0c00330

IMPORTANT NOTE: You are advised to consult the publisher's version (publisher's PDF) if you wish to cite from it. Please check the document version below.

Document Version
Publisher's PDF, also known as Version of record

Publication date:
2020

Link to publication in University of Groningen/UMCG research database

Citation for published version (APA):
Yang, L., Ge, L., Zhou, Q., Jurczak, K. M., & van Rijn, P. (2020). Decoupling the Amplitude and Wavelength of Anisotropic Topography and the Influence on Osteogenic Differentiation of Mesenchymal Stem Cells Using a High-Throughput Screening Approach. *ACS Applied Bio Materials*, *3*(6), 3690-3697. https://doi.org/10.1021/acsabm.0c00330

Copyright
Other than for strictly personal use, it is not permitted to download or to forward/distribute the text or part of it without the consent of the author(s) and/or copyright holder(s), unless the work is under an open content license (like Creative Commons).

The publication may also be distributed here under the terms of Article 25fa of the Dutch Copyright Act, indicated by the “Taverne” license. More information can be found on the University of Groningen website: https://www.rug.nl/library/open-access/self-archiving-pure/taverne-amendment.

Take-down policy
If you believe that this document breaches copyright please contact us providing details, and we will remove access to the work immediately and investigate your claim.

This is an open access article published under a Creative Commons Non-Commercial No Derivative Works (CC-BY-NC-ND) Attribution License, which permits copying and redistribution of the article, and creation of adaptations, all for non-commercial purposes.

ACS AUTHORCHOICE

ACS APPLIED BIO MATERIALS

www.acsabm.org

Article

Decoupling the Amplitude and Wavelength of Anisotropic Topography and the Influence on Osteogenic Differentiation of Mesenchymal Stem Cells Using a High-Throughput Screening Approach

Liangliang Yang, Lu Ge, Qihui Zhou, Klaudia Malgorzata Jurczak, and Patrick van Rijn*

Cite This: *ACS Appl. Bio Mater.* 2020, 3, 3690–3697

Read Online

ACCESS | Metrics & More | Article Recommendations | Supporting Information

ABSTRACT: High-throughput screening (HTS) methods based on anisotropically topography gradients have been broadly used to investigate the interactions between cells and biomaterials. However, few studies focus on the optimum parameters of topography for osteogenic differentiation because the structures of topography are complex with multiple combinations of parameters. In this study, we developed polydimethylsiloxane (PDMS)-based wrinkled topography gradients (amplitudes between 144 and 2854 nm and wavelengths between 0.91 and 13.62 μm) and decoupled the wavelength and amplitude via imprinting lithography and shielded plasma oxidation. The PDMS wrinkle gradient was then integrated with the bottomless 96-well plate to constitute the wrinkled HTS platform, which consists of 70 different wrinkle parameters. From the in vitro culture of bone marrow stem cells, it was observed that aligned topography has an important influence on the macroscopic cell behavior (i.e., cell area, elongation, and nucleus area). Furthermore, the optimum wrinkle parameter (wavelength: 1.91 μm; amplitude: 360 nm) for osteogenic differentiation of stem cells was determined via this screening plate approach. This screening platform is not only beneficial for a better understanding of the interactions between topography and biomaterials but also advances the development of bone tissue engineering developments.

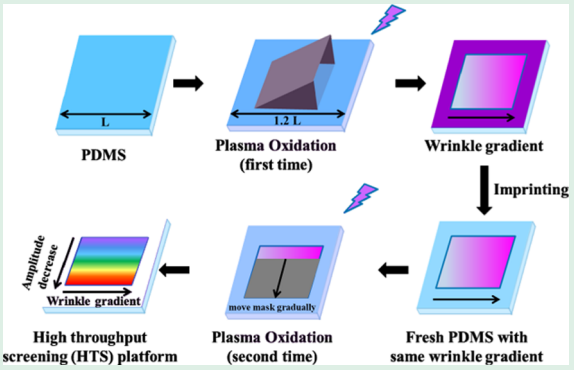

KEYWORDS: *high-throughput screening, topographical gradient, stem cell, osteogenic differentiation, materiobiology*

1. INTRODUCTION

The key for the development of biomaterials in tissue engineering and regenerative medicine is the ability to use the physicochemical properties to control cell behavior.[1] Mesenchymal stem cells (MSCs) are an interesting cell type because of their autologous availability,[2] capacity to differentiate into multilineage potential (adipogenic, osteogenic, and chondrogenic differentiation),[2] and low immunogenic reaction by allogeneic hosts.[3] Therefore, controlling the differentiation behavior of MSCs is vital in many biological aspects such as bone regeneration.[4] MSCs could perceive the physical or topographical signals from the extracellular matrix (ECM) and respond to these signals and thereby influence cell responses, including adhesion, proliferation, migration, and differentiation.[5−11] The surface topography significantly affects cell behavior through contact guidance,[12] and the cell is able to sense such surface parameters between 10 nm and 100 μm.[13,14] Previous studies demonstrate that enhanced osteogenic differentiation stimulated by topography is caused by the increased formation of focal adhesion, activation of RhoA/Rock signaling pathway,[15,16] and the regulation of microRNA.[5] Furthermore, researchers also revealed that topography-induced integrin-linked kinase (ILK)/β-catenin pathway,[17] ILK/extracellular signal-regulated kinase 1/2 and ILK/p38,[18] and crosstalk between focal adhesion kinase/mitogen-activated protein kinase and ILK/β-catenin pathways[19] facilitate osteogenesis of stem cells.

In vivo, the ECM of most tissues, for instance, bone, tendon, and nerve, has anisotropic architectures composed of aligned nano-/microscaled structures.[20−23] There are various studies focused on the impact of anisotropic structures on the differentiation of stem cells. Kukumberg et al.[24] investigated the influence of anisotropic topography on the endothelial differentiation of MSCs and found that the 1.8 μm diameter convex microlens pattern combined with the vascular

Received: March 25, 2020
Accepted: May 6, 2020
Published: May 6, 2020

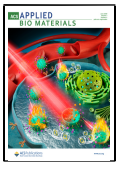

Downloaded via UNIV GRONINGEN on February 23, 2021 at 12:01:12 (UTC).
See https://pubs.acs.org/sharingguidelines for options on how to legitimately share published articles.

© 2020 American Chemical Society

https://dx.doi.org/10.1021/acsabm.0c00330
ACS Appl. Bio Mater. 2020, 3, 3690–3697

endothelial growth factor was found to be most efficient for differentiation. Tan and co-workers[25] prepared a multi-architecture chip with different topographical structures and parameters to study the neuron differentiation of neural progenitor cells. The data revealed that the different combinations of parameters (grating, spacing, height) triggered cells toward varied degree of neuronal differentiation. These studies illustrate that topography with specific parameters enhances osteogenic and neuronal differentiation. However, it should be noted that many of these studies use topographies with parameters that are relatively chosen arbitrarily, which provided significant yet limited information. Furthermore, the structures mentioned above are extremely complex with various combinations of topography parameters (i.e., groove, ridge, and pitch); therefore, the parameters that play an important role in guiding cell behavior are not exactly known unless these parameters are decoupled. Therefore, in order to better understand the relevant topographical features, it is essential to systematically change one parameter to determine its influence on cellular behaviors.

Surface topographical gradients provide an ideal platform to study cell behavior in a high-throughput screening (HTS) manner. This method is time- and cost-efficient and minimizes systematic or methodological errors.[26] Furthermore, the platform can screen for the optimum topographical parameters for promoting specific cellular processes.[26−29] Previously, our group studied cell contact guidance using micro-/nanotopographical gradients and found that the parameter of topography has an essential effect on various cell activities, for example, cell orientation, elongation, migration, and differentiation.[30−37] The wavy-like wrinkle structure is a powerful tool for engineering nano- and microstructures in a cost-effective way.[38,39] In addition, the grating structure consists of sharp corners or edges that may not be supportive for cells.[38,39] Furthermore, wrinkles consist of two parameters, namely, wavelength and amplitude, and these two parameters have always been coupled in previous studies. However, by decoupling the wavelength and amplitude, specific insights in individual contributions of topography parameters may be gained.

In this study, we hypothesize that both wavelength and pitch contribute to topography-mediated cell stimulation. To investigate these individual contributions of topography parameters, we prepared a HTS platform consisting of 70 different combinations of wavelengths and amplitudes in one 96-well plate, following the work of der Boon et al.[40] By sequentially preparing aligned topography gradients via a silicone stretch-oxidation-release method and imprinting lithography, followed by selective amplitude reduction using plasma oxidation for different durations, the amplitude and wavelength were decoupled, and the whole substrate was integrated into standardized well-plate technology. Using the multiparameter topography well plate, the optimum wavelength/amplitude combination for osteogenesis of human bone marrow-derived MSCs (hBM-MSCs) was investigated. The wrinkle parameters were characterized by atomic force microscopy (AFM). hBM-MSCs were seeded to study the influences of wrinkle parameters on macroscopic cell behavior (i.e., cell area, cell elongation, and nucleus area) and osteogenic differentiation, which was examined by immunofluorescence staining of alkaline phosphate (ALP) and alizarin red staining, respectively. This HTS platform facilitates the understanding of the relationships between the biointerface and biological behavior, and the screening capability provides great potential for the designing of biomaterials.

2. METHODS

2.1. Polydimethylsiloxane Film Preparation and Wrinkle Gradient Formation. Polydimethylsiloxane (PDMS) film and wrinkle gradient were prepared as described previously.[30,41] Briefly, the PDMS substrate was fabricated by mixing the liquid PDMS precursor and curing agent (Sylgard 184, Dow Corning) with a weight ratio of 10:1. The mixture was degassed for 15 min to remove air bubbles and cured at 70 °C overnight. For the wrinkled gradient, the cured PDMS (10.5 × 9 cm) was stretched uniaxially to 120% of the original length, and then the surface was covered with a right-angled triangular prism mask (10 × 8 cm, with an angular aperture of 30°) and oxidized in air plasma (Plasma Activate Flecto 10 USB, maximum intensity) for 650 s at 25 mTorr. After oxidation, a glassy layer (SiO_2) is formed on the surface of the substrate, and because of the shielded role of the mask, the thickness of the SiO_2 layer decreases from the most exposed side (mask opening) to the least exposed side. The mask dimensions provide control over the oxidation gradient development. Afterward, the strain was released, inducing the formation of wrinkled gradients, and the wrinkle wavelength and amplitude increased from the lowest oxidized region (closed side) to the highest oxidized region (open side of the mask). All substrates were further oxidized for 10 min under the pressure of 100−150 mTorr to make the surface completely oxidized, which was beneficial for the imprinting process.

2.2. Imprinting. The fabricated PDMS wrinkle gradient was used as a mold, and a fresh mixture of precursor and curing agent (weight ratio of 10:1) was poured onto it, followed by overnight curing at 70 °C. Afterward, the mold was removed, and the newly prepared substrate with wrinkle gradients was used for further study.

2.3. Decoupling the Wavelength and Amplitude. After imprinting, the fresh PDMS membrane has again the elastomeric properties rather than the oxidized surface of the mold, while the same wrinkle structures as the mold are still present. Then, the soft PDMS membrane was oxidized with a flat mask for different times (0, 5, 10, 20 s, 1, 2, and 10 min). Longer plasma oxidation time resulted in more reduction in the amplitude of the wrinkles. After that, the PDMS substrate was imprinted again to ensure that the surface chemical and mechanical properties are the same for all samples. The substrates were further oxidized by plasma at 500 mTorr for 1 min and used for integrating it into the well plate. The flat substrate (10:1 for the ratio of the precursor and curing agent) was prepared and oxidized with the same condition of plasma mentioned above to confirm that all the substrates have the same chemical and mechanical properties.

2.4. PDMS Surface Characterization. Topography images were obtained by an atomic force microscope (Nanoscope V Dimension 3100 microscope, Veeco, United States) performed with tapping mode in the air (DNP-10 tip). The wavelength and amplitude of the wrinkle gradient were determined by NanoScope Analysis software.

2.5. Well Plate Embedding. The bottomless 96-well plate embedded with the PDMS membrane was prepared as described previously.[40] Briefly, the samples for wrinkle gradients were cut into sizes of 9.6 × 7.5 cm to cover wells A1−H1 through columns 1−10 of the plate (Greiner Bio-One no. 655101), and column 11 was sacrificed to connect the wrinkle gradient with column 12, which acts as a flat control (1.5 × 7.5 cm) (Figure S1). Then, the area of the plate bottom was coated with a liquid mixture of precursor and curing agent, and the plate was put into the oven for the mixture to form a glue-like state. The two substrates were carefully placed on top of the glue and pressed firmly to ensure that a good connection is made. At last, ∼32 g of the PDMS mixture was poured on top of the bottom. Samples were cured at 70 °C for 3 h to seal the bottom.

2.6. Cell Culture. hBM-MSCs obtained from Lonza were used for the experiments. hBM-MSCs were cultured in a proliferation medium comprising Alpha modified Eagle's medium (Gibco), 10% fetal bovine serum (Gibco), 0.1% ascorbic acid 2-phosphate (Sigma), and 1%

https://dx.doi.org/10.1021/acsabm.0c00330
ACS Appl. Bio Mater. 2020, 3, 3690−3697

penicillin/streptomycin (Gibco). Cells were cultured at 37 °C in the presence of 5% CO_2. The medium was refreshed every 3 days, and cells were detached with trypsin and harvested at 80% confluence. hBM-MSCs of passage 4 were used for all of the experiments.

2.7. Immunostaining. The embedded well plate was sterilized with 75% ethanol and then washed with Dulbecco's phosphate-buffered saline (DPBS). Afterward, 2500 cells of hBM-MSCs were seeded in each well. For immunostaining, hBM-MSCs seeded on the different topographical patterns were fixed in 3.7% paraformaldehyde (PFA, Sigma) solution for 20 min at room temperature and subsequently permeabilized with 0.5% Triton X-100 (Sigma) solution for 3 min and incubated with 5% bovine serum albumin (Sigma) in PBS for 30 min. Then, the cells were stained with primary anti-ALP antibody (Developmental Hybridoma Bank, B4-78, 1:100) for 1 h and secondary rhodamine Red-X-conjugated goat-anti-mouse antibody (Jackson Immunolab, 1:100), 4′6-diamidino-2-phenylindole (DAPI), and TRITC-phalloidin for 1 h. Finally, the images were taken with TissueFaxs (Tissue-Gnostics GmbH, Vienna, Austria). Cell area and nucleus area were determined by TissueQuest. Cell elongation was calculated as the ratio between the length of the cell major axis and length of the minor axis (for the quantification of cell area, nucleus area, and cell elongation, ≥60 cells for each sample and three independent experiments were analyzed).

2.8. Osteogenic Differentiation of MSCs. hBM-MSCs were seeded onto substrates at a cell density of 2500 cells/well. All plates were stored in an incubator at 37 °C, 5% CO_2, and after 24 h, the medium was exchanged for osteogenic differentiation medium (OM) composed of growth medium and osteogenic supplements [10 mM glycerophosphate (Sigma) and 100 nM dexamethasone (Sigma)] for 14−21 days. The culture medium was replaced every 3 days. ALP and nucleus staining were performed by the method mentioned above.

To further examine osteogenesis, mineralization of the ECM was stained with alizarin red after 21 days under OM. The samples were washed twice with DPBS and fixed with 4% PFA for 15 min, and then 0.1% alizarin red solution was added into the wells. After 30 min, the wells were washed with DPBS to remove the excess of alizarin red solution. For quantitative analysis, the cultures stained with alizarin red were destained with 10% cetylpyridinum chloride in 10 mM sodium phosphate buffer for 30 min to release the bound calcium. The supernatant was collected, and a microplate reader (BMG LABTECH, Offenburg, Germany) was used to measure the absorbance at 540 nm. The values were normalized for the cell numbers for each well, and the cell number was quantified by the nucleus stained with DAPI through TissueQuest.

2.9. Statistics. All values are expressed as the mean ± standard deviation (SD). Origin 9.0 software was used to perform statistical analysis. One-way analysis of variance (ANOVA) was used with Tukey's test to identify differences between groups: $*P < 0.05$, $**P < 0.01$, and $***P < 0.001$.

3. RESULTS AND DISCUSSION

3.1. Preparation of Wrinkle Gradient and Surface Characterization. The preparation process for the topographical gradient is illustrated in Figure 1. During the process, the PDMS substrate was uniaxially stretched and plasma-oxidized with the surface being shielded using a right-angled triangular prism mask. After releasing the strain, the wrinkle gradient was formed, and the wrinkle parameters were tunable by changing the oxidation time, angle of the mask, as well as pressure. The wrinkle size increased with increasing plasma exposure occurring from the least exposed side to the most exposed side, and the largest wrinkle dimensions were observed when extending to the area without a mask (fully exposed to plasma). It has to be noted that the amplitude and wavelength are always coupled, and larger wavelengths are correlated with higher amplitudes.

The surface features after imprinting (before the second oxidation treatment) were characterized by AFM, as shown in

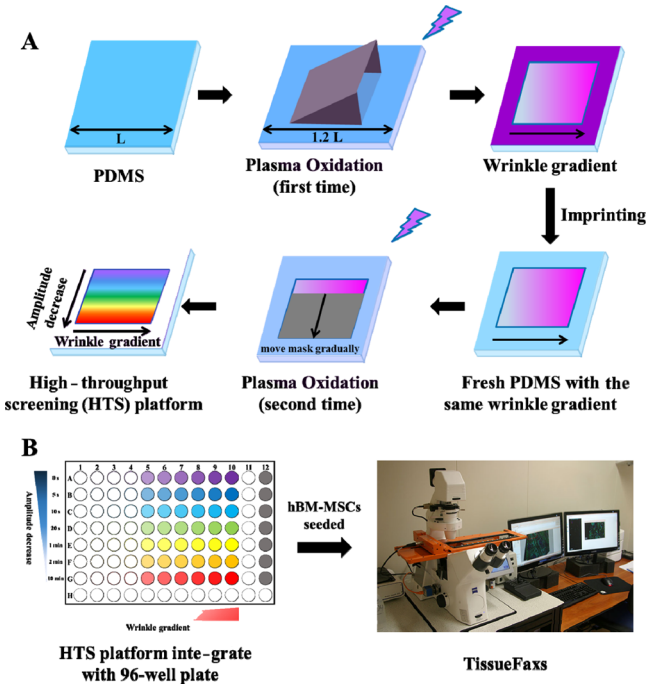

Figure 1. (A) Schematic diagrams of the formation of a HTS platform by air plasma oxidation. The PDMS membrane was stretched uniaxially to 120% of the original length, followed by covering with a mask and oxidized in air plasma (first time). After oxidation, releasing the strain induced the formation of wrinkled gradients. After imprinting, the new soft PDMS membrane was oxidized to decrease the amplitude or decouple the wavelength and amplitude. (B) The HTS platform was integrated with the bottomless 96-well plate and seeded with hBM-MSCs to induce osteogenic differentiation. The immunofluorescence staining for ALP (an important marker for osteogenesis) was imaged with TissueFaxs.

Figure 2A. The anisotropic topography gradients were prepared with amplitudes ranging from 144 to 2854 nm and wavelengths between 0.91 and 13.62 μm, as shown in Figure 2B,C where the numbers depict the column number of the final position in the 96-well plate. There is not a linear increase for the development of wavelength and amplitude but a steeper increase (after the eighth position) toward the end of the gradient. However, for the wrinkle, the wavelength and amplitude are always coupled. In order to determine the optimum parameter promoting the osteogenic differentiation of hBM-MSCs, it is important to decouple these two parameters.

3.2. Decoupling the Amplitude via Plasma Oxidation. The surface of the substrate formed a bioglass-like (SiO_2) layer after the oxidation process.[30] Therefore, it is crucial for the mold to be imprinted into pristine PDMS before the second time plasma oxidation. The amplitude of the wrinkles was found to decrease when applying the second time plasma oxidation and longer time generated the lower amplitude (Figure 3). The oxidation provides stiffening and surface cross-linking. The combination of surface cross-linking, loss of the organic segments of PDMS due to overoxidation, and the transformation from an elastomeric to a more organized phase most likely induces tension on the surface. As a result of this tension, the wrinkles are affected, and it was found that particularly the amplitude was influenced the most, resulting in reduction of the amplitude, while the wavelength was found to remain the same. Therefore, in this way, the wavelength and

https://dx.doi.org/10.1021/acsabm.0c00330
ACS Appl. Bio Mater. 2020, 3, 3690−3697

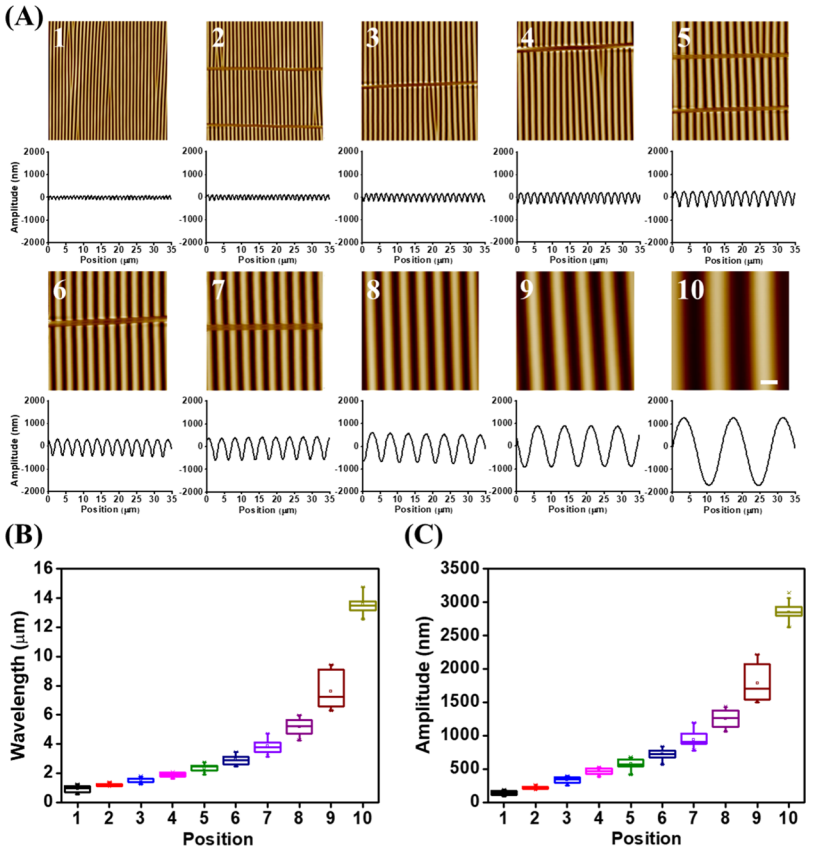

Figure 2. (A) Representative AFM images and amplitude curves of wrinkles along the gradient after imprinting. The number (1, 2, ..., 10) in the AFM image stands for the column number in the 96-well plate. Quantification analysis of wavelength (B) and amplitude (C) of the created wrinkle gradient. ≥30 wrinkles for each sample and three independent imprints were analyzed. Scale bar represents 5 μm.

amplitude were decoupled, and control over the amount of amplitude reduction was achieved by altering the oxidation time. By shielding the rows sequentially, a high-throughput platform was prepared by moving the mask gradually (Figure 1A).

As shown in Figure 3, after the plasma oxidation for different times, the wrinkle retained its shape, but as observed from the height profiles, the amplitude decreased after the oxidation. Furthermore, a longer oxidation time resulted in a lower amplitude (Figure 3A). For column 1, the amplitude decreased from 144 nm to 6 nm, while column 10 displayed a reduction in amplitude from 2854 to 833 nm (Figure 3B). Every row had the same wavelength development, while the wavelength was fixed within a column. However, within a column, the amplitudes gradually decreased from row A to G. This approach provides the foundation for the HTS platform consisting of 70 different combinations of wavelengths and amplitudes. The substrate with a 9.6 cm length and a 7.5 cm width was chosen (Figure S1) to cover the area from column 1 to the middle of column 11. A flat control was placed in column 12. The integration of the substrates into a 96-well plate ensures proper handling; because no variations in surface location are possible, a gradient is highly susceptible to small differences in location. An additional important aspect is that it allows the technology to be used more broadly as the well plate technology is compatible with the standardized equipment and able to be used by all without prior specific training.

3.3. Macroscopic Behavior of hBM-MSCs Modulated by the Wrinkle Wavelength and Amplitude. Cell elongation and orientation are crucial features for many anisotropic tissue functions.[42] Using the screening platform composed of different wavelengths and amplitudes as culture substrates, we investigated the influence on the morphology and orientation of hBM-MSCs. For this purpose, cells were cultured for 1 day on the substrates. As shown in Figure 4A (the image for all the wells is displayed in Figure S2), cell behavior was analyzed by TissueFaxs. From the fluorescence imaging of cells within the various wells, it is clearly shown that the cells became more oriented and elongated with increasing wavelength. For instance, compared to position G1, cells cultured on position G10 showed high elongation and orientation along the long axis of the wrinkles. There were similar trends for other rows. More importantly, for the same wavelength, with the decrease of amplitude, the morphology of cells changed from elongated and oriented to a more random shape (e.g., A1−G1).

Furthermore, the cell area, cell elongation, and nucleus area were determined by TissueQuest. A two-dimensional (2D) heat map representation originating from the analysis of every well within the well plate showed the cell area, cell elongation, and nucleus area after 24 h of culture (Figures 4B,C and S3). The cell spreading was visualized by analyzing the phalloidin-stained fiber actin. As shown in Figure 4B, the cell area is greatly influenced by the amplitude of wrinkles. The cell area increased with decreasing amplitude, which was observed in column 9 where the average cell area of 3651 μm^2 at the low amplitude side decreased to 1062 μm^2 at the higher amplitude side. This decrease was observed for all wavelengths and indicates that the lower amplitude of the wrinkle enhances the cell spreading and the higher amplitude suppresses it.

https://dx.doi.org/10.1021/acsabm.0c00330
ACS Appl. Bio Mater. 2020, 3, 3690−3697

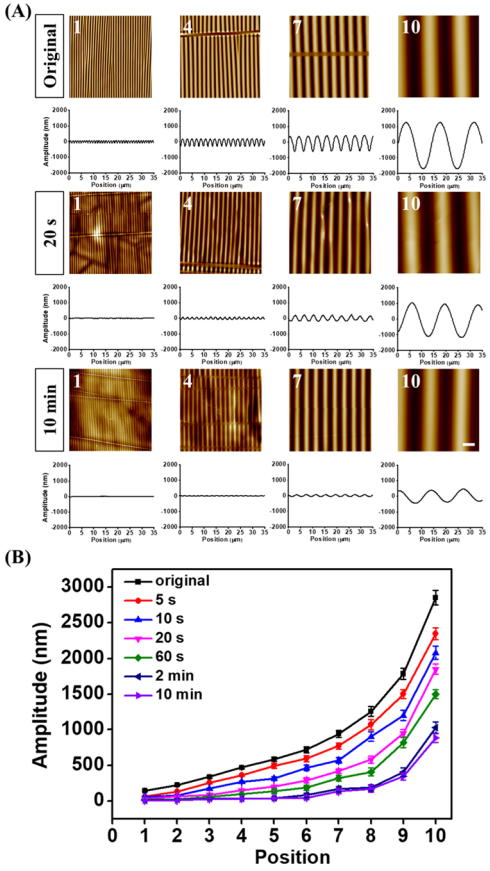

Figure 3. (A) Representative AFM images taken after imprinting and amplitude curves of the wrinkles along the gradient after different times (0, 20 s, 10 min) of plasma oxidation. (B) Variation curve of amplitude after the second time plasma oxidation. ≥30 wrinkles for each sample and three independent substrates were analyzed. Scale bar represents 5 μm.

The cell aspect ratio (C_{AR}) is an essential characterization of cell shape.[43] Moreover, the differentiation behavior of stem cells could be dramatically affected by AR.[43−45] As shown in Figure 4C, AR was adjusted synergistically by the wavelength and amplitude. With the decrease of amplitude, there has been a steep drop in the C_{AR}, suggesting that a higher amplitude enhances the C_{AR} and a lower amplitude suppresses it. Furthermore, the C_{AR} increased with increasing wavelength, and the largest C_{AR} was found on position A10 (AR: 11.83) which was the position with the highest wavelength and amplitude. Several studies reported that different values for the C_{AR} have a great effect on the osteogenic and adipogenic differentiation of MSCs. Kilian and co-workers[45] examined three cases of C_{AR} (1, 1.5, 4) and found that adipogenesis decreased with C_{AR} and observed a monotonic increase of osteogenesis with increasing C_{AR}. Ding et al.[44] studied six cases of AR (1, 1.5, 2, 4, 8, 16) and found the same conclusion for adipogenic differentiation and 2 is the optimal for osteogenesis. Moreover, Ding et al.[43] revealed that C_{AR} itself is an inherent factor for guiding the lineage commitment of MSCs regardless of chemical factors. Although these studies have provided valuable information, it is important to note that most studies focused on the C_{AR} with discrete values, not in a continuous way. In contrast, in this study, cells showed varied C_{AR} ranging from 3.42 to 11.83, which is advantageous to explore the influence of different C_{AR} on the fate commitment of stem cells.

The nucleus size is closely associated with nuclear function and cell differentiation.[46] It was found that cells exhibited a larger nucleus area on the HTS platform with smaller amplitude (Figure S3). Cells grown on the small wrinkle side showed an increase in the nucleus area per cell with decreasing amplitude going from the average nucleus area of 234 μm^2 at the low amplitude side to 139 μm^2 at the high amplitude side. Similarly, the cells showed the same trend when they were on the larger wrinkle side. Taken together, these results indicate that the amplitude of wrinkles has a significant influence on the cell spreading and morphology. Moreover, the amplitude and wavelength have a combined role for these phenomena.

3.4. Optimum Parameter of Wrinkles for the Osteogenesis of hBM-MSCs. To identify the optimum wrinkle parameter for osteogenic differentiation, hBM-MSCs were cultured in OM for 14 and 21 days. The osteogenic

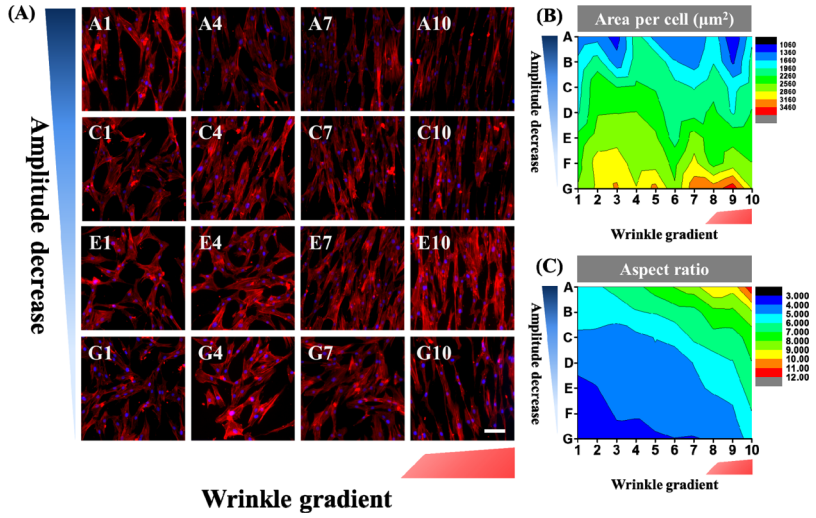

Figure 4. (A) Representative fluorescent images of hBM-MSCs cultured on different wells in a 96-well plate. TRITC-phalloidin (red) and DAPI (blue) were used to stain F-actin and cell nucleus, respectively. Scale bar represents 100 μm. 2D heat map representations of cell area (B) and cell aspect ratio (C) for the HTS platform (≥60 cells were analyzed). Each experiment was performed in triplicate.

https://dx.doi.org/10.1021/acsabm.0c00330
ACS Appl. Bio Mater. 2020, 3, 3690−3697

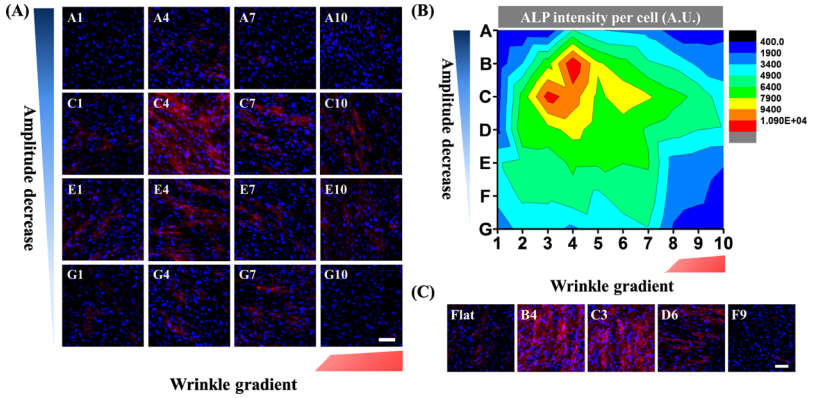

Figure 5. (A) Immunofluorescence staining of ALP for hBM-MSCs grown on the HTS platform cultured in OM for 14 days. Nucleus (blue) and ALP (red) were stained. (B) 2D heat map representations of the ALP intensity which was normalized by the cell number (at least 50 cells were analyzed), and each experiment was performed in triplicate. (C) Immunofluorescence staining of ALP for hBM-MSCs grown on flat, B4, C3, D6, and F9, cultured in OM for 14 days. Nucleus (blue) and ALP (red) were stained. Scale bar represents 100 μm.

differentiation was evaluated by the immunofluorescence staining of ALP and alizarin red staining.

3.4.1. ALP Expression. ALP activity is a marker for the osteogenesis of stem cells[47] and used to evaluate the osteogenic differentiation of hBM-MSC.[48] To visualize the differentiation on the HTS platform, the cells were stained with the antibody against ALP after 2 weeks of culture. Figure 5A shows that hBM-MSCs displayed varied fluorescence density of ALP on the HTS platform. With the decrease of amplitude, a gradual rise in the intensity of ALP was observed, followed by a drop, suggesting that the expression of ALP is significantly influenced by the amplitude of wrinkles. For the wrinkle gradient (X-axis), the ALP expression displayed a similar trend as mentioned above. The expression was quantified by evaluating the intensity of fluorescence (Figure 5B). The fluorescence intensity is normalized to the cell number, which indicates a good agreement with the qualitative analysis. The optimum positions on the HTS topography well plate for osteogenic differentiation were B4 and C3, and the corresponding parameters of wrinkles were W: 1.91 μm/A: 360 nm for B4 and 1.55 μm/173 nm for C3. Furthermore, ALP staining for representative positions (i.e., flat, B4, C3, D6, and F9) are displayed in Figure 5C.

3.4.2. Alizarin Red Staining. Mineralization is an important indicator of osteoblasts, and the nodules can be stained with alizarin red, which is commonly used to evaluate the osteogenesis of stem cells.[49] From the results of ALP staining, the positions B4, C3, D6, F9 (corresponding to the 96-well plate entries), and flat were selected, and the uniform substrates (suitable for a 24-well plate) corresponding to the features of each of these positions were prepared for further study. Larger uniform substrates were prepared as the liquid handling (repetitive washing) within the 96-well plate was found to disturb the alizarin red-stained nodules, resulting in a less accurate read-out. For immunofluorescence staining, this aspect was not a problem.

After 21 days in OM, the mineralized nodules on the substrates were stained with alizarin red (Figure 6A). hBM-MSCs grown on the substrate B4 showed the highest expression of mineralization compared to those on the substrates C3 and D6, while the expression on F9 and flat was rather minimal. The value of OD at 540 nm was measured to further quantify the mineralization of hBM-MSCs. As shown in Figure 6B, the highest OD_{540} was obtained for cells cultured

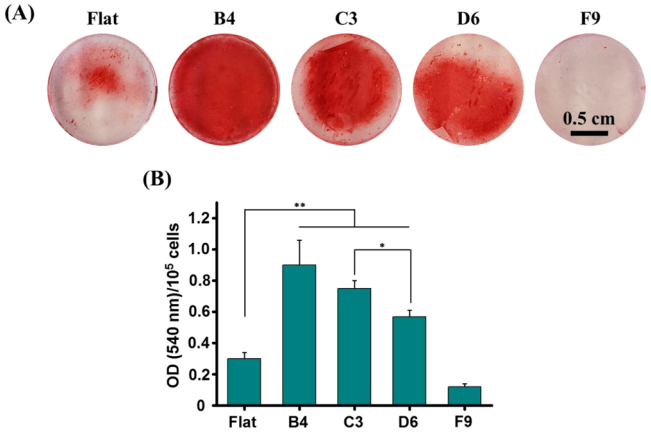

Figure 6. (A) Representative images of calcium stained with alizarin red for hBM-MSCs cultured in OM for 21 days. (B) Quantification of the extent of mineralization, normalized by the cell number, and each experiment was performed in triplicate. Data are shown as mean ± SD, and $^{**}P < 0.01$, $^{*}P < 0.05$. Scale bar represents 0.5 cm.

on B4, followed by those on C3, which suggests the best osteogenic differentiation. The value was significantly lower for 9F and flat. The mineralization results are consistent with the ALP expression. Taken together, these results indicate that the optimum parameter for the osteogenic differentiation of stem cells is B4 (W: 1.91 μm/A: 360 nm) and that the 96-well plate with double topography parameter alterations is a valuable tool to identify topography-mediated cell responses.

4. CONCLUSIONS

The HTS platform consisting of 70 different combinations of wavelengths and amplitudes in a 96-well plate was successfully prepared. The key feature is the possibility to decouple the wavelength and amplitude and thereby allows in identifying the contribution to cell behavior of both parameters. The results of the cell culture in vitro show that the cell area, elongation, and nucleus area were significantly influenced by the varied wrinkle parameters. Furthermore, hBM-MSCs showed different osteogenic differentiation capacities on the platform, and the optimum parameter for the wrinkle features was identified to be W: 1.91 μm/A: 360 nm (B4). The platform with a broad topography spectrum is an elegant substrate for the investigation of topography directing fate commitment of

https://dx.doi.org/10.1021/acsabm.0c00330
ACS Appl. Bio Mater. 2020, 3, 3690−3697

stem cells. Also, this versatile platform employed herein that is usable by all with standard approaches and equipment provides a powerful strategy for improving the development of biomaterials for bone tissue engineering.

■ ASSOCIATED CONTENT

Supporting Information

The Supporting Information is available free of charge at https://pubs.acs.org/doi/10.1021/acsabm.0c00330.

Dimensions and orientation of the PDMS substrates embedded with the bottomless 96-well plate; fluorescent images of hBM-MSCs grown in a 96-well plate after 1 day; and quantified nucleus area for the cells grown on the HTS platform (PDF)

■ AUTHOR INFORMATION

Corresponding Author

Patrick van Rijn − *University of Groningen, University Medical Center Groningen, Department of Biomedical Engineering-FB40 Groningen, 9713 AV Groningen, The Netherlands;* orcid.org/0000-0002-2208-5725; Email: p.van.rijn@umcg.nl

Authors

Liangliang Yang − *University of Groningen, University Medical Center Groningen, Department of Biomedical Engineering-FB40 Groningen, 9713 AV Groningen, The Netherlands*

Lu Ge − *University of Groningen, University Medical Center Groningen, Department of Biomedical Engineering-FB40 Groningen, 9713 AV Groningen, The Netherlands;* orcid.org/0000-0002-5782-4823

Qihui Zhou − *Department of Stomatology, Institute for Translational Medicine, The Affiliated Hospital of Qingdao University, Qingdao University, 266003 Qingdao, China;* orcid.org/0000-0003-2474-4197

Klaudia Malgorzata Jurczak − *University of Groningen, University Medical Center Groningen, Department of Biomedical Engineering-FB40 Groningen, 9713 AV Groningen, The Netherlands*

Complete contact information is available at: https://pubs.acs.org/10.1021/acsabm.0c00330

Author Contributions

The manuscript was written through contributions of all authors.

Notes

The authors declare the following competing financial interest(s): Conflict of Interest P.v.R also is co-founder, scientific advisor, and share-holder of BiomACS BV, a biomedical oriented screening company. The authors declare no other competing interests.

■ ACKNOWLEDGMENTS

The authors are very grateful for financial support of the China Scholarship Council (nos. 201608310113 and 201707720058). This work was supported by the UMCG Microscopy and Imaging Center (UMIC) sponsored by NWO-grant 40-00506-98-9021. The authors acknowledge Klaas Sjollema for assistance with the TissueFaxs microscope.

■ REFERENCES

(1) Vega, S. L.; Arvind, V.; Mishra, P.; Kohn, J.; Sanjeeva Murthy, N.; Moghe, P. V. Substrate Micropatterns Produced by Polymer Demixing Regulate Focal Adhesions, Actin Anisotropy, and Lineage Differentiation of Stem Cells. *Acta Biomater.* **2018**, *76*, 21−28.

(2) Pittenger, M. F. Multilineage Potential of Adult Human Mesenchymal Stem Cells. *Science* **1999**, *284*, 143−147.

(3) Xu, G.; Zhang, L.; Ren, G.; Shi, Y.; Yuan, Z.; Zhang, Y.; Zhao, R. C. Immunosuppressive Properties of Cloned Bone Marrow Mesenchymal Stem Cells IL-17 Signaling View Project IL-17C and Colon Cancer View Project Immunosuppressive Properties of Cloned Bone Marrow Mesenchymal Stem Cells. *Cell Res.* **2007**, *17*, 240−248.

(4) Caplan, A. I. Adult Mesenchymal Stem Cells for Tissue Engineering versus Regenerative Medicine. *J. Cell. Physiol.* **2007**, *213*, 341−347.

(5) Yang, J.; McNamara, L. E.; Gadegaard, N.; Alakpa, E. V.; Burgess, K. V.; Meek, R. M. D.; Dalby, M. J. Nanotopographical Induction of Osteogenesis through Adhesion, Bone Morphogenic Protein Cosignaling, and Regulation of MicroRNAs. *ACS Nano* **2014**, *8*, 9941−9953.

(6) Teo, B. K. K.; Wong, S. T.; Lim, C. K.; Kung, T. Y. S.; Yap, C. H.; Ramagopal, Y.; Romer, L. H.; Yim, E. K. F. Nanotopography Modulates Mechanotransduction of Stem Cells and Induces Differentiation through Focal Adhesion Kinase. *ACS Nano* **2013**, *7*, 4785−4798.

(7) Zhang, S.; Ma, B.; Liu, F.; Duan, J.; Wang, S.; Qiu, J.; Li, D.; Sang, Y.; Liu, C.; Liu, D.; Liu, H. Polylactic Acid Nanopillar Array-Driven Osteogenic Differentiation of Human Adipose-Derived Stem Cells Determined by Pillar Diameter. *Nano Lett.* **2018**, *18*, 2243−2253.

(8) Li, L.; Yang, S.; Xu, L.; Li, Y.; Fu, Y.; Zhang, H.; Song, J. Nanotopography on titanium promotes osteogenesis via autophagy-mediated signaling between YAP and β-catenin. *Acta Biomater.* **2019**, *96*, 674−685.

(9) Stanton, A. E.; Tong, X.; Yang, F. Extracellular Matrix Type Modulates Mechanotransduction of Stem Cells. *Acta Biomater.* **2019**, *96*, 310−320.

(10) Dalby, M. J.; Gadegaard, N.; Oreffo, R. O. C. Harnessing Nanotopography and Integrin-Matrix Interactions to Influence Stem Cell Fate. *Nat. Mater.* **2014**, *13*, 558−569.

(11) Schaap-Oziemlak, A. M.; Kühn, P. T.; Van Kooten, T. G.; Van Rijn, P. Biomaterial-Stem Cell Interactions and Their Impact on Stem Cell Response. *RSC Adv.* **2014**, *4*, 53307−53320.

(12) Kim, J.; Kim, H. N.; Lim, K.-T.; Kim, Y.; Pandey, S.; Garg, P.; Choung, Y.-H.; Choung, P.-H.; Suh, K.-Y.; Chung, J. H. Synergistic Effects of Nanotopography and Co-Culture with Endothelial Cells on Osteogenesis of Mesenchymal Stem Cells. *Biomaterials* **2013**, *34*, 7257−7268.

(13) Dalby, M.; Riehle, M. O.; Johnstone, H.; Affrossman, S.; Curtis, A. S. G. Investigating the limits of filopodial sensing: a brief report using SEM to image the interaction between 10 nm high nanotopography and fibroblast filopodia. *Cell Biol. Int.* **2004**, *28*, 229−236.

(14) Dunn, G. A.; Heath, J. P. A New Hypothesis of Contact Guidance in Tissue Cells. *Exp. Cell Res.* **1976**, *101*, 1−14.

(15) Seo, C. H.; Jeong, H.; Feng, Y.; Montagne, K.; Ushida, T.; Suzuki, Y.; Furukawa, K. S. Micropit Surfaces Designed for Accelerating Osteogenic Differentiation of Murine Mesenchymal Stem Cells via Enhancing Focal Adhesion and Actin Polymerization. *Biomaterials* **2014**, *35*, 2245−2252.

(16) Seo, C. H.; Furukawa, K.; Montagne, K.; Jeong, H.; Ushida, T. The Effect of Substrate Microtopography on Focal Adhesion Maturation and Actin Organization via the RhoA/ROCK Pathway. *Biomaterials* **2011**, *32*, 9568−9575.

(17) Wang, W.; Zhao, L.; Wu, K.; Ma, Q.; Mei, S.; Chu, P. K.; Wang, Q.; Zhang, Y. The role of integrin-linked kinase/β-catenin pathway in the enhanced MG63 differentiation by micro/nano-textured topography. *Biomaterials* **2013**, *34*, 631−640.

(18) Wang, W.; Liu, Q.; Zhang, Y.; Zhao, L. Involvement of ILK/ERK1/2 and ILK/P38 Pathways in Mediating the Enhanced

Osteoblast Differentiation by Micro/Nanotopography. *Acta Biomater.* **2014**, *10*, 3705−3715.
(19) Niu, H.; Lin, D.; Tang, W.; Ma, Y.; Duan, B.; Yuan, Y.; Liu, C. Surface Topography Regulates Osteogenic Differentiation of MSCs via Crosstalk between FAK/MAPK and ILK/β-Catenin Pathways in a Hierarchically Porous Environment. *ACS Biomater. Sci. Eng.* **2017**, *3*, 3161−3175.
(20) Wegst, U. G. K.; Bai, H.; Saiz, E.; Tomsia, A. P.; Ritchie, R. O. Bioinspired Structural Materials. *Nat. Mater.* **2015**, *14*, 23−36.
(21) Yin, Z.; Chen, X.; Chen, J. L.; Shen, W. L.; Hieu Nguyen, T. M.; Gao, L.; Ouyang, H. W. The Regulation of Tendon Stem Cell Differentiation by the Alignment of Nanofibers. *Biomaterials* **2010**, *31*, 2163−2175.
(22) Engelmayr, G. C.; Cheng, M.; Bettinger, C. J.; Borenstein, J. T.; Langer, R.; Freed, L. E. Accordion-like Honeycombs for Tissue Engineering of Cardiac Anisotropy. *Nat. Mater.* **2008**, *7*, 1003−1010.
(23) Georgiou, M.; Bunting, S. C. J.; Davies, H. A.; Loughlin, A. J.; Golding, J. P.; Phillips, J. B. Engineered Neural Tissue for Peripheral Nerve Repair. *Biomaterials* **2013**, *34*, 7335−7343.
(24) Kukumberg, M.; Yao, J. Y.; Neo, D. J. H.; Yim, E. K. F. Microlens Topography Combined with Vascular Endothelial Growth Factor Induces Endothelial Differentiation of Human Mesenchymal Stem Cells into Vasculogenic Progenitors. *Biomaterials* **2017**, *131*, 68−85.
(25) Tan, K. K. B.; Tann, J. Y.; Sathe, S. R.; Goh, S. H.; Ma, D.; Goh, E. L. K.; Yim, E. K. F. Enhanced Differentiation of Neural Progenitor Cells into Neurons of the Mesencephalic Dopaminergic Subtype on Topographical Patterns. *Biomaterials* **2015**, *43*, 32−43.
(26) Faia-Torres, A. B.; Guimond-Lischer, S.; Rottmar, M.; Charnley, M.; Goren, T.; Maniura-Weber, K.; Spencer, N. D.; Reis, R. L.; Textor, M.; Neves, N. M. Differential Regulation of Osteogenic Differentiation of Stem Cells on Surface Roughness Gradients. *Biomaterials* **2014**, *35*, 9023−9032.
(27) Kim, D.-H.; Han, K.; Gupta, K.; Kwon, K. W.; Suh, K.-Y.; Levchenko, A. Mechanosensitivity of Fibroblast Cell Shape and Movement to Anisotropic Substratum Topography Gradients. *Biomaterials* **2009**, *30*, 5433−5444.
(28) Kim, D.-H.; Seo, C.-H.; Han, K.; Kwon, K. W.; Levchenko, A.; Suh, K.-Y. Guided Cell Migration on Microtextured Substrates with Variable Local Density and Anisotropy. *Adv. Funct. Mater.* **2009**, *19*, 1579−1586.
(29) Beijer, N. R. M.; Vasilevich, A. S.; Pilavci, B.; Truckenmüller, R. K.; Zhao, Y.; Singh, S.; Papenburg, B. J.; de Boer, J. TopoWellPlate: A Well-Plate-Based Screening Platform to Study Cell-Surface Topography Interactions. *Adv. Biosyst.* **2017**, *1*, 1700002.
(30) Zhou, Q.; Castañeda Ocampo, O.; Guimarães, C. F.; Kühn, P. T.; Van Kooten, T. G.; Van Rijn, P. Screening Platform for Cell Contact Guidance Based on Inorganic Biomaterial Micro/Nanotopographical Gradients. *ACS Appl. Mater. Interfaces* **2017**, *9*, 31433−31445.
(31) Liguori, G. R.; Zhou, Q.; Liguori, T. T. A.; Barros, G. G.; Kühn, P. T.; Moreira, L. F. P.; van Rijn, P.; Harmsen, M. C. Directional Topography Influences Adipose Mesenchymal Stromal Cell Plasticity: Prospects for Tissue Engineering and Fibrosis. *Stem Cells Int.* **2019**, *2019*, 5387850.
(32) Almonacid Suarez, A. M.; Zhou, Q.; Rijn, P.; Harmsen, M. C. Directional topography gradients drive optimum alignment and differentiation of human myoblasts. *J. Tissue Eng. Regener. Med.* **2019**, *13*, 2234−2245.
(33) Abagnale, G.; Sechi, A.; Steger, M.; Zhou, Q.; Kuo, C.-C.; Aydin, G.; Schalla, C.; Müller-Newen, G.; Zenke, M.; Costa, I. G.; van Rijn, P.; Gillner, A.; Wagner, W. Surface Topography Guides Morphology and Spatial Patterning of Induced Pluripotent Stem Cell Colonies. *Stem Cell Rep.* **2017**, *9*, 654−666.
(34) Ge, L.; Yang, L.; Bron, R.; Burgess, J. K.; Van Rijn, P. Topography-Mediated Fibroblast Cell Migration Is Influenced by Direction, Wavelength, and Amplitude. *ACS Appl. Bio Mater.* **2020**, *3*, 2104−2116.
(35) Yang, L.; Gao, Q.; Ge, L.; Zhou, Q.; Warszawik, E. M.; Lai, K. W. C.; van Rijn, P. Topography Induced Stiffness Alteration of Stem Cells Influences Osteogenic Differentiation. *Biomater. Sci.* **2020**, *8*, 2638.
(36) Yang, L.; Ge, L.; Zhou, Q.; Mokabber, T.; Pei, Y.; Bron, R.; Van Rijn, P. Biomimetic Multiscale Hierarchical Topography Enhances Osteogenic Differentiation of Human Mesenchymal Stem Cells. *Adv. Mater. Interfaces* **2020**, 2000385.
(37) Yang, L.; Jurczak, K. M.; Ge, L.; Rijn, P. High-Throughput Screening and Hierarchical Topography-Mediated Neural Differentiation of Mesenchymal Stem Cells. *Adv. Healthcare Mater.* **2020**, 2000117.
(38) Choi, Y.-J.; Park, S. J.; Yi, H.-G.; Lee, H.; Kim, D. S.; Cho, D.-W. Muscle-Derived Extracellular Matrix on Sinusoidal Wavy Surfaces Synergistically Promotes Myogenic Differentiation and Maturation. *J. Mater. Chem. B* **2018**, *6*, 5530−5539.
(39) Song, K. H.; Park, S. J.; Kim, D. S.; Doh, J. Sinusoidal wavy surfaces for curvature-guided migration of T lymphocytes. *Biomaterials* **2015**, *51*, 151−160.
(40) der Boon, T. A. B.; Yang, L.; Li, L.; Córdova Galván, D. E.; Zhou, Q.; Boer, J.; Rijn, P. Well Plate Integrated Topography Gradient Screening Technology for Studying Cell-Surface Topography Interactions. *Adv. Biosyst.* **2020**, *4*, 1900218.
(41) Lee, J. S.; Hong, H.; Park, S. J.; Lee, S. J.; Kim, D. S. A Simple Fabrication Process for Stepwise Gradient Wrinkle Pattern with Spatially-Controlled Wavelength Based on Sequential Oxygen Plasma Treatment. *Microelectron. Eng.* **2017**, *176*, 101−105.
(42) Prager-Khoutorsky, M.; Lichtenstein, A.; Krishnan, R.; Rajendran, K.; Mayo, A.; Kam, Z.; Geiger, B.; Bershadsky, A. D. Fibroblast Polarization Is a Matrix-Rigidity-Dependent Process Controlled by Focal Adhesion Mechanosensing. *Nat. Cell Biol.* **2011**, *13*, 1457−1465.
(43) Yao, X.; Peng, R.; Ding, J. Effects of Aspect Ratios of Stem Cells on Lineage Commitments with and without Induction Media. *Biomaterials* **2013**, *34*, 930−939.
(44) Peng, R.; Yao, X.; Ding, J. Effect of Cell Anisotropy on Differentiation of Stem Cells on Micropatterned Surfaces through the Controlled Single Cell Adhesion. *Biomaterials* **2011**, *32*, 8048−8057.
(45) Kilian, K. A.; Bugarija, B.; Lahn, B. T.; Mrksich, M. Geometric Cues for Directing the Differentiation of Mesenchymal Stem Cells. *Proc. Natl. Acad. Sci. U.S.A.* **2010**, *107*, 4872−4877.
(46) Liu, X.; Liu, R.; Cao, B.; Ye, K.; Li, S.; Gu, Y.; Pan, Z.; Ding, J. Subcellular Cell Geometry on Micropillars Regulates Stem Cell Differentiation. *Biomaterials* **2016**, *111*, 27−39.
(47) Kim, I. G.; Hwang, M. P.; Du, P.; Ko, J.; Ha, C.-w.; Do, S. H.; Park, K. Bioactive Cell-Derived Matrices Combined with Polymer Mesh Scaffold for Osteogenesis and Bone Healing. *Biomaterials* **2015**, *50*, 75−86.
(48) Li, J.; Mou, X.; Qiu, J.; Wang, S.; Wang, D.; Sun, D.; Guo, W.; Li, D.; Kumar, A.; Yang, X.; Li, A.; Liu, H. Surface Charge Regulation of Osteogenic Differentiation of Mesenchymal Stem Cell on Polarized Ferroelectric Crystal Substrate. *Adv. Healthcare Mater.* **2015**, *4*, 998−1003.
(49) Qiu, J.; Li, J.; Wang, S.; Ma, B.; Zhang, S.; Guo, W.; Zhang, X.; Tang, W.; Sang, Y.; Liu, H. TiO2Nanorod Array Constructed Nanotopography for Regulation of Mesenchymal Stem Cells Fate and the Realization of Location-Committed Stem Cell Differentiation. *Small* **2016**, *12*, 1770−1778.

https://dx.doi.org/10.1021/acsabm.0c00330
ACS Appl. Bio Mater. 2020, 3, 3690−3697